Applied Catalysis B: Environmental 232 (2018) 86–92

Contents lists available at ScienceDirect

Applied Catalysis B: Environmental

journal homepage: www.elsevier.com/locate/apcatb

# Improving methane selectivity of photo-induced $CO_2$ reduction on carbon dots through modification of nitrogen-containing groups and graphitization

Zhi Liu[a,b], Zhijian Wang[b,*], Shaojun Qing[b], Nannan Xue[a,b], Suping Jia[b], Li Zhang[b], Li Li[b], Na Li[b], Liyi Shi[a,*], Jiazang Chen[b,*]

[a] Department of Chemistry, Shanghai University, Shanghai 200444, China
[b] State Key Laboratory of Coal Conversion, Institute of Coal Chemistry, Chinese Academy of Sciences, Taiyuan 030001, China

ARTICLE INFO

*Keywords:*
Carbon dots
$CO_2$ reduction
Photocatalysis
Nitrogen doping
Methane

ABSTRACT

The photocatalytic performance of carbon dots is strongly related to surface modifications and graphitization. Herein, we show that carbon dots without metal loaded can serve as an efficient photocatalyst for reducing $CO_2$. The conjugate carbon great π could stabilize the photogenerated electrons, which turned out to improve the separation of the photogenerated electron-hole pairs and can kinetically promote interfacial reaction. Besides, the strong chemisorption of the nitrogen-containing groups on the carbon dots to the CO would help to further conversion of the intermediate in the demonstrated $CO_2$ photo-reduction systems. As a result of these merits, the highly graphitized carbon dots prepared from graphene oxide with plenty of nitrogen-containing groups exhibit 74.8% electronic selectivity of methane. This strategy provides an important requirement for designing of $CO_2$ photocatalysts.

## 1. Introduction

Carbon dots (CDs) have gradually become a rising star as a new category of metal-free nanomaterials for their unique optoelectronic properties, such as broad-band optical absorption, bright fluorescence emissions, low photobleaching, reliable chemical inertness, favorable photoinduced electron transfer properties, and tailorable surface chemistry [1–7]. Most researchers recognize the work on CDs-based photocatalysts by Li and co-workers as a milestone [8]. Since then, the adhibition of CDs in photocatalysis has increased explosively, with the function of CDs as catalysts or co-catalysts causing extensive concern.

In fact, the extraordinary properties of CDs are highly relevant to the carbon dot structure [9–11]. For example, the graphitization has significant impact on their light harvesting ability [12]. CDs with nitrogen doped can improve the efficiency of charge transfer reactions [13,14]. High upward band bending induced by the C═O and COOH groups on the surface of CDs would facilitate the separation of the electron-hole pairs [15]. The surface energy and chemisorption properties have played a key role in the energy conversion and transfer, and also in managing the rate, selectivity and overpotential of redox reaction on the photocatalyst surface [16,17].

Solar driven reduction of $CO_2$ into energetic molecules (e.g., $CH_4$, CO, $CH_3OH$, and HCOOH) is a desirable chemical process to convert exhaustless solar energy into securable clean chemical energy which is considered as an ultimate solution to the growing environmental challenge on carbon sequestration [18–20]. The versatile CDs have exhibited multiplicate functions in photocatalytic $CO_2$ reduction. When $Cu_2O$ nanospheres are coated with CDs, the CDs/$Cu_2O$ composite presents lower reflectance than $Cu_2O$ which means higher light restriction ability, and the CDs can lightly lower the apparent bandgap of the whole composite with1.96 ± 0.02 eV rather than 2.2 eV indicating more usage of the sunlight [21]. Surface-functionalized CDs could harvest visible photons, and the aqueous solubility of the catalysts enables photoreduction under more desirable homogeneous reaction conditions to facilitate the photocatalytic process [22]. However, up to now, CDs-based $CO_2$ reduction photocatalysts reported all contain metals or metal oxides. In this work, the intrinsic catalysis of CDs, without metal loaded, on photocatalytic $CO_2$ reduction was investigated. The CDs with nitrogen-containing groups and high graphitization degree show high photocatalytic activity and methane selectivity. This is attributed to outstanding separation of the photogenerated electron-hole pair. Furthermore, the stronger chemisorption property, which is induced by nitrogen-containing groups, determines the high selectivity towards methane.

* Corresponding authors.
*E-mail addresses:* wangzhijian@sxicc.ac.cn (Z. Wang), shiliyi@shu.edu.cn (L. Shi), chenjiazang@sxicc.ac.cn (J. Chen).

https://doi.org/10.1016/j.apcatb.2018.03.045
Received 21 December 2017; Received in revised form 10 March 2018; Accepted 14 March 2018
Available online 16 March 2018
0926-3373/ 

## 2. Experimental

### 2.1. Preparation of amorphous carbon dots (ACDs)

#### 2.1.1. GH-i-ACDs

Glucose (10.35 g) was dissolved in distilled water (184 mL) to form a clear solution. Concentrated HCl (46 mL) was added to the solution of glucose. Then the mixture was transferred into an inner irradiation-type Pyrex reactor. The reactants were irradiated at high-pressure Hg lamp (300 W) for 12 h. The temperature of the mixture was maintained at 20 °C with a cool, flowing water. After that, the solution was dialyzed for 3 days with a dialysis tube (molecular weight 3500) to remove the excess precursors and resulting small molecules. The obtained aqueous suspension of GH-i-ACDs was kept at 4 °C for further use.

#### 2.1.2. GN-u-ACDs

GN-u-ACDs was synthesized using one-step ultrasonic-assisted method according to earlier report [23]. Glucose (9 g) was dissolved in distilled water (50 mL) to form a clear solution. NaOH (2 g) was added to the solution of glucose. Then the mixture was treated by an ultrasonic wave (100 W, 40 KHz) for 1 h. HCl was dropwise added into the crude sample obtained from glucose/NaOH in order to adjust to PH = 7. After that, the solution was dialyzed for 3 days with a dialysis tube (molecular weight 3500) to remove the excess precursors and resulting small molecules, and finally the product was obtained. The obtained aqueous suspension of GN-u-ACDs was kept at4 °C for further use.

### 2.2. Preparation of graphitized carbon dots with nitrogen-containing groups (GCDs)

#### 2.2.1. GO-h-GCDs

Graphene oxide (GO) was prepared by the modified Hummers' method from natural graphite powder [12]. The graphite powder (3 g) and $NaNO_3$ (1.5 g) were introduced to concentrated $H_2SO_4$ (69 mL) in an ice-bath. $KMnO_4$ (9 g) was added gradually under stirring, so that the temperature of the mixture was kept below 20 °C. The reaction was then heated to 35 °C and stirred for 24 h. Then, distilled water (8 mL) was slowly added to the mixture, followed by stirring the mixture at 98 °C for 15 min. The suspension was further diluted to 500 mL and cooled to room temperature. The reaction was terminated by adding $H_2O_2$ (25 mL) under stirring. Multiple washing with distilled water was conducted and the graphene oxide sample was obtained by drying the precipitate of the final slurry at 60 °C for 48 h.

GO-h-GCDs were prepared via ultrasonic-assisted hydrothermal treatment of the GO. In a typical synthesis, GO (0.4 g) was dispersed in distilled water (200 mL) and sonicated (100 W, 40 KHz) for 8 h. Then the mixture was transferred into three 100 mL Teflon-lined autoclave and kept heated at 180 °C for 10 h. The GO-h-GCDs were collected by removing larger particles through filtering using a cylindrical filtration membrane filter (0.22 μm of pore size). The obtained aqueous suspension of GO-h-GCDs was kept at 4 °C for further use.

#### 2.2.2. CNT-h-GCDs

CNT-h-GCDs had the same synthesis pathway with GO-h-GCDs, except that natural graphite powders were replaced by multi-walled carbon nanotubes as carbon sources.

### 2.3. Photocatalytic performance of the obtained CDs

$CO_2$ reduction reactions were accomplished using a closed system with an inner irradiation-type Pyrex reactor. A suitable amount of CDs was added into Pyrex reactor. The CDs solution was further diluted to 220 mL. The mixed solution was $CO_2$ saturated via $CO_2$ purging before the reaction and was irradiated by high-pressure Hg lamp (300 W). The temperature of the mixed was maintained at 20 °C with cool flowing water. The products formation rate was measured via gas chromatography.

### 2.4. Measurement and characterization

To acquire the UV–Vis absorption spectrum, the CDs solutions were put in a 1-cm quartz curette and analyzed using a Shimadzu UV-3600 UV–vis-NIR spectrophotometer at room temperature. TEM images were performed using a JEOL JEM-2010 microscope with an accelerating voltage of 200 kV. Fourier transform infrared spectroscopy (FTIR) was carried out on a Nicolet Magna-IR 550-II spectrometer with KBr pallets. PL emission spectra were performed using a Hitachi F-7000 FL spectrophotometer. XPS was obtained using a Thermo ESCALAB 250 XPS spectrometer with Al Kα ($h\nu$ = 1486.6 eV) radiation. To eliminate the effect of sample surface charging the shift of the XPS peak of carbon (C1s whose binding energy is 284.6 eV) was used. The isotopic experiment for $CO_2$ reduction by using $^{13}CO_2$ was performed with a Perfect Light PLS-SXE 300 and mass spectrometer. The baseline of mass spectrometer sampled in air with the limit of equipment. After three hours reaction, products were tested three times in succession and took the average in order to avoid operation error. (Molar mass setting: 16 = $CH_4$; 17 = $^{13}CH_4$; 28 = $CO/N_2$; 29 = $^{13}CO$, 44 = $CO_2$; 45 = $^{13}CO_2$). PL lifetime was studied at room temperature using a commercial laser-flash photolysis spectrometer (Edinburgh Instruments LP920-KS), a photomultiplier tube (Hamamatsu R928), a gated CCD (Princeton Instruments, Pl-MAX ICCD camera), and a digital oscilloscope (Tektronix TDS-3012C).

CDs electrodes for electrochemical analysis were prepared by dropping the CDs solution (about 10 mg CDs) onto an FTO glass and dried in air. The CDs electrodes were subjected to electrochemical analysis in saturated $CO_2$ solution with a Pt sheet as the counter electrode and saturated Ag/AgCl as the reference electrode on a CHI 760D electrochemical analyzer. The potential of the working electrode was constant at 0.45 V under intermittent illumination with a period of 10 s each.

The carbon dioxide-temperature-programmed desorption ($CO_2$-TPD) measurement was carried out on Autochem tp5080 chemisorption analyzer (Xianquan Tianjin, China). Firstly, the sample was pre-treated in He at 300 °C for 1 h. Then, the adsorption of $CO_2$ was done at 50 °C and subsequently flushed in He (50 mL/min) for 1 h. The $CO_2$desorption was conducted at temperature increasing from 50 to 950 °C in He flow at a heating rate of 10 °C/min. The carbon monoxide-temperature-programmed desorption (CO-TPD) was measured by the same instrument. About 60 mg of sample in a quartz tube was heated up to 200 °C (10 °C/min) under He, and then purged at the same temperature for 1 h. After cooled down to 50 °C, a flow of Ar containing 10%CO was pre-adsorbed on the catalyst at 50 °C for 30 min to ensure saturated adsorption. After that, the sample was swept with He for 30 min in order to purge the gaseous and physisorbed CO from the sample surface, and then the sample was heated to 900 °C at a heating rate of 10 °C/min. The released CO was determined with a gas chromatograph equipped with a TCD detector.

The electronic selectivity of products is calculated as follows:

$$ESm = \frac{Mm \times 8}{Mm \times 8 + Mh \times 2 + Mc \times 2} \times 100\%$$

$$ESh = \frac{Mh \times 2}{Mm \times 8 + Mh \times 2 + Mc \times 2} \times 100\%$$

$$ESc = \frac{Mm \times 2}{Mm \times 8 + Mh \times 2 + Mc \times 2} \times 100\%$$

Where $ES_m$, $ES_h$, $ES_c$ are the electronic selectivity of methane, hydrogen and carbon monoxide, respectively. And Mm, Mh, Mc is the molar yield of methane, hydrogen and carbon monoxide, respectively.

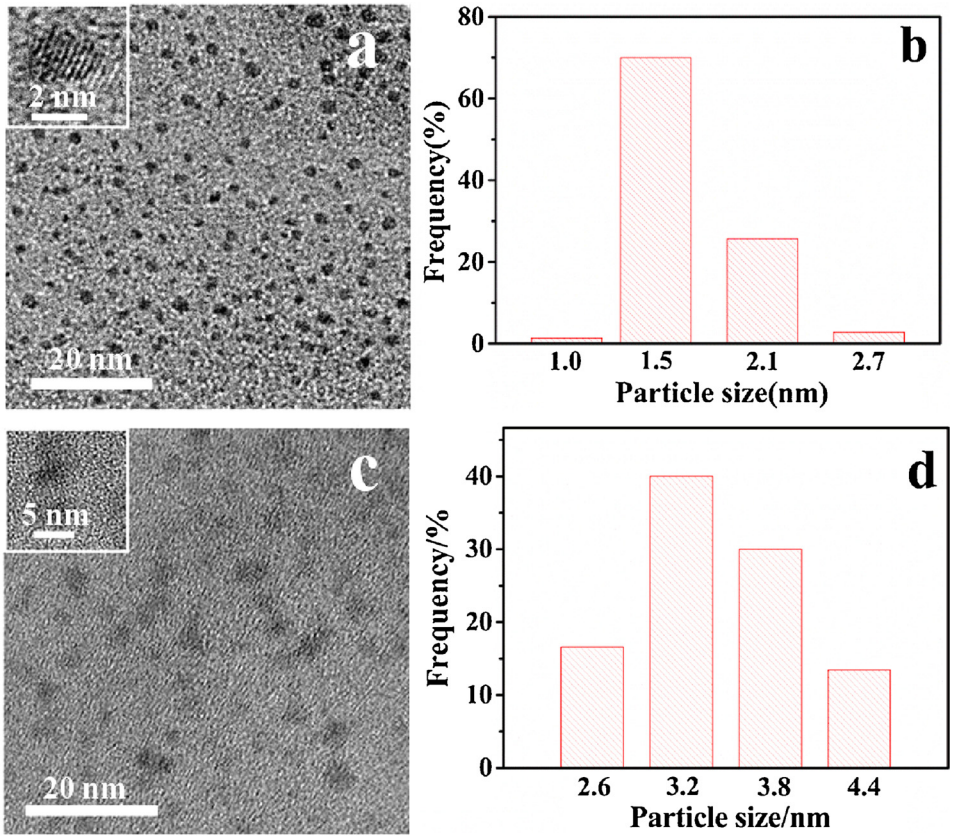


**Fig. 1.** (a) TEM images of GO-h-GCDs (inset is the HRTEM image) and (b) the corresponding particle size distribution histogram; (c) TEM image of GH-i-ACDs (inset is the HRTEM image) and (d) the corresponding particle size distribution histogram.

## 3. Results and discussion

The uniform dispersion of CDs was confirmed from TEM micrographs and particle size distribution histograms (Figs. 1 and S1). The CDs were spherical in shape with a narrow size distribution less than 3 nm. The inset in Figs. 1a and S1a show that GO-h-GCDs and CNT-h-GCDs were observed to be quasi-crystalline carbon particles with a slight indistinct appearance of lattice, while the absence of any discernible lattice structure from Figs. 1c and S1c suggests an amorphous nature for GH-i-ACDs and GN-u-ACDs. The crystallization was also characterized by XRD (Fig. 2). As shown in Fig. 2, a broad reflection peak appeared between 24.7° and 28.4° corresponding to highly disordered carbon atoms [3,24,25]. This peak broadened due to the small size effect and shifted to low degree because of different oxidation degree [26]. Additionally, the particular peak of GCDs at about 43.4° corresponded to the hexagonal carbon (power diffraction file PDF No. 26-1083). The differences might be induced by the synthetic methods. Top-down approaches aim to physically exfoliate large carbon structures into quantum-size CDs with clean surfaces and high crystallinity (GCDs), while the ACDs coming from bottom-up methods possess abundant doping states and surface functional groups. Hexagonal arrangement of carbon atoms is the fundamental units of two-dimensional graphene and one-dimensional carbon nanotubes. This two-dimensional $sp^2$ hybridised graphene has been considered as the foundation for carbon materials of all other dimensionalities [6,27]. CDs are the mixture of $sp^2$ and $sp^3$ hybridised carbon that determine their intrinsic and extrinsic properties.

To clarify the nature of the synthesized CDs, UV–vis spectra was plotted as shown in Fig. 3. The UV–vis spectra of CDs in water shows the first absorption peak near 230 nm, corresponding to the ordered $\pi \rightarrow \pi^*$ transition of aromatic $sp^2$ domains [28]. The optical gaps between the highest occupied molecular orbital (HOMO) and the lowest unoccupied molecular orbital (LUMO) of the CDs were determined according to Tauc plot with a linear extrapolation (Fig. S2). The CDs did not have a uniform oxidation level that they cannot reveal sharp

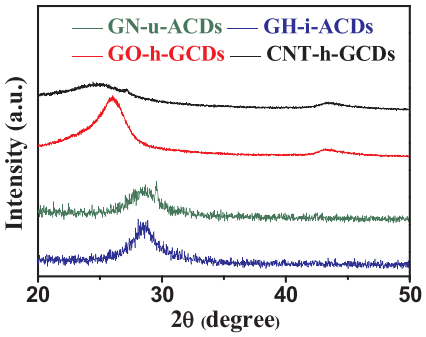


**Fig. 2.** XRD images of GO-h-GCDs, CNT-h-GCDs, GN-u-ACDs and GH-i-ACDs.

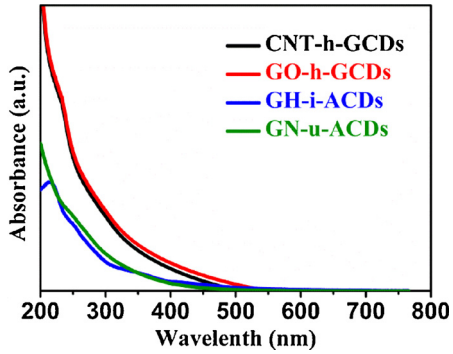


**Fig. 3.** UV–vis spectra of GO-h-GCDs, CNT-h-GCDs, GN-u-ACDs and GH-i-ACDs.

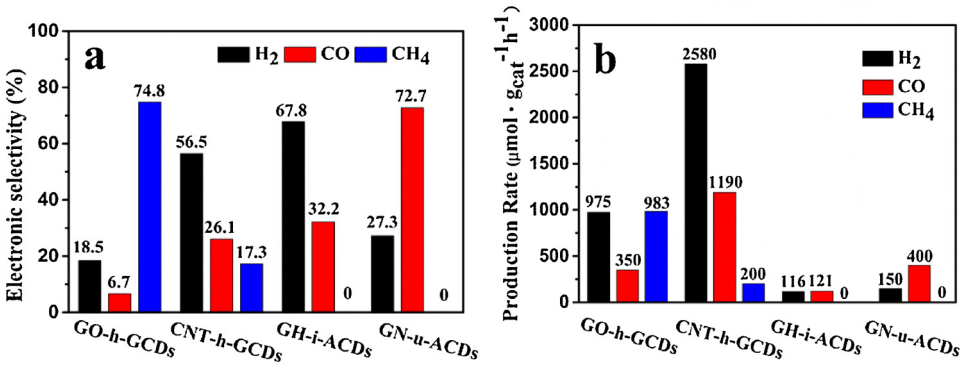


**Fig. 4.** Comparison of the electronic selectivity (a) and generation rate (b) after a 5 h photocatalytic reduction of $CO_2$.

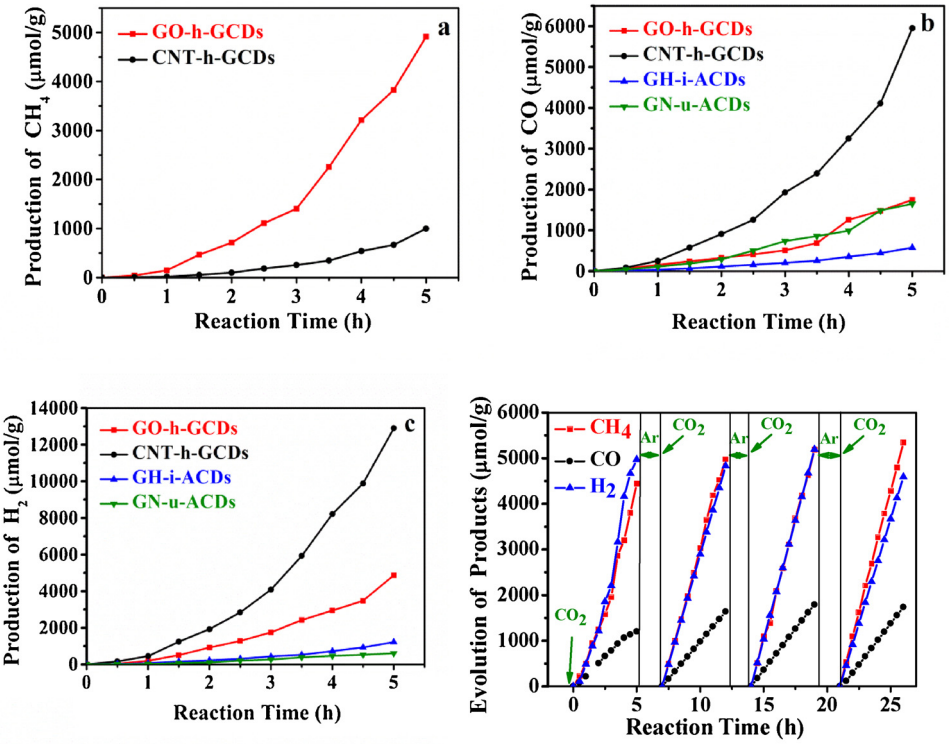


**Fig. 5.** The time courses of $CH_4$ (a), CO (b), $H_2$ (c) evolution, and recycling stability tests of GO-h-GQDs over 20 h (d).

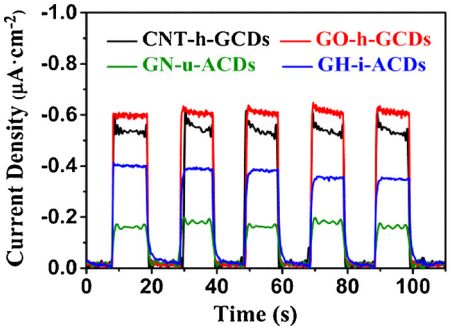


**Fig. 6.** Transient photocurrent responses of GO-h-GCDs, CNT-h-GCDs, GN-u-ACDs and GH-i-ACDs.

absorption edges. A rough minimum HOMO-LUMO gap range was found over 2.34, 2.38, 2.75 and 2.89 eV for CNT-h-GCDs, GO-h-GCDs, GH-i-ACDs and GN-u-ACDs, respectively. Previous studies showed that the calculated HOMO-LUMO gap of a cluster of 20 aromatic rings is about 2 eV, which increases to approximately 7 eV in a benzene ring through DFT calculations [29]. Thus, it is believed that the smaller bandgap of GCDs is likely related to much bigger $sp^2$ clusters of aromatic rings.

The photocatalysis of $CO_2$ reduction of the prepared CDs was investigated under irradiation of a high-pressure Hg lamp. Fig. 4 shows a comparison of the production rate and electron selectivity obtained after 5 h of photocatalytic reduction of $CO_2$. As can be seen, the photocatalysis products of all CDs contained$H_2$ and CO. At the same time, GCDs also showed a wonderful ability to reduce $CO_2$ into $CH_4$, especially GO-h-GCDs with an electronic selectivity towards $CH_4$ of 74.8%. No other products were detected by either GC or GC–MS analyses. Isotope experiment was conducted with $^{13}CO_2$, which indicated that 95.94% $^{13}CH_4$ came from $^{13}CO_2$ and a small amount of $CH_4$was from GO-h-GCDs (Fig. S3). The reduction of ion current of 28, represented CO and $N_2$, stemmed from switching air (baseline) to products. The rapid loss of the concentration of $N_2$ covered up very small increment of the concentration of CO. And the enormous increase in $^{13}CO$ demonstrated that the most carbon atoms in CO was from $CO_2$.Furthermore, GCDs showed much higher photocatalytic activity than ACDs (Fig. 4b). Fig. 5a–c shows the time courses of evolution of $CH_4$, CO and $H_2$ on CDs

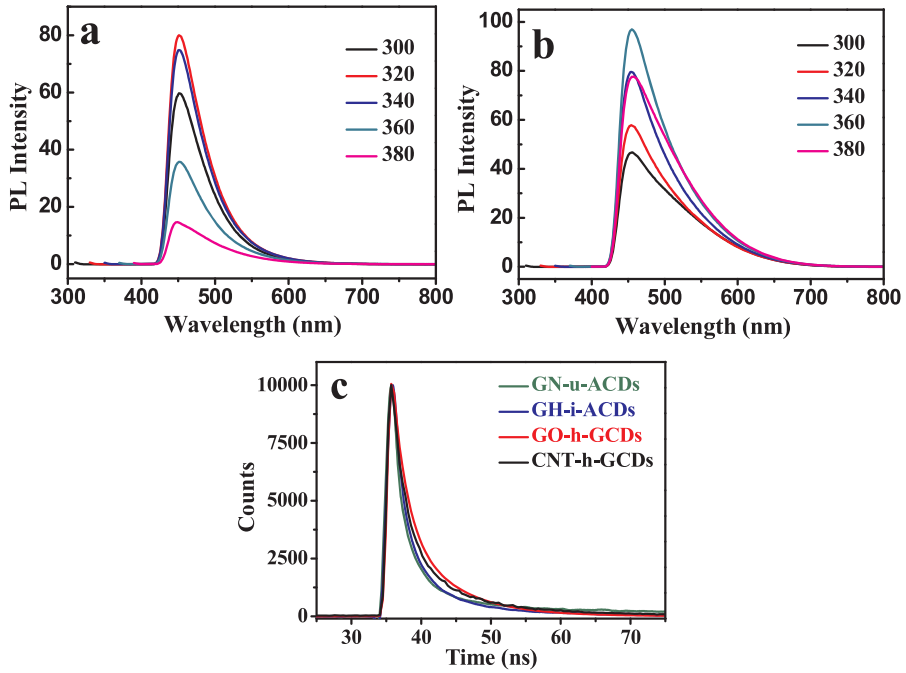


**Fig. 7.** PL emission spectra where excitation wavelength shifts from 300 to 380 nm for GO-h-GCDs (a), GH-i-ACDs (b). (c) Time-resolved photoluminescence spectra for CDs.

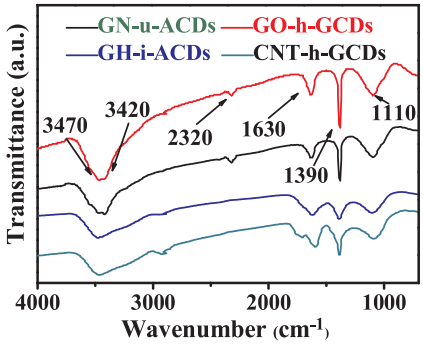


**Fig. 8.** FTIR spectra of GO-h-GCDs, CNT-h-GCDs, GN-u-ACDs and GH-i-ACDs.

under UV irradiation without any sacrificial agents. To determine the stability of GO-h-GCDs, the cyclic stability experiment was carried out. We can see that after 20 h photocatalytic $CO_2$ reduction, the evolution rate and production selectivity shows unobservable variation (Fig. 5d), indicating a favourable stability of the CD photocatalysts.

For photocatalysis applications, the photo-induced electron-hole separation is considerably important. Transient photocurrent analysis is a diffusely used typical method to research the electron-hole separation effect. Fig. 6 shows significant currents were generated when the light source was switched on. The date points shown were separated by 10 s for each light on and off. It was worth noting that the response time to both the on and the off was short, which indicated that it was a quick response and well-defined increase. Moreover, once exposed to light, the current appears to be constant. Additionally, GCDs showed a higher photocurrent intensity than ACDs, and this distinct enhancement in photocurrent indicated intensive separation of photogenerated electron-hole pairs for GCDs. The total electronic density of the GCDs was determined by large $sp^2$ clusters, meanwhile the charge transfer properties were also dependent on the spatial distribution of the smaller fragments, which may act as bridges between large ones [29,30]. It is believed that both the smaller and the larger $sp^2$ clusters of graphitized GCDs contribute to this remarkable improvement over the transport of carrier.

The PL behavior of CDs was shown in Figs. 7 and Fig. S4. The π and π* electronic levels of the $sp^2$ clusters lie within the bandgap of σ and σ*states of the $sp^3$ matrix and are strongly localized [31,32], thus the PL peak positions of CDs were found to remain constant around 450 nm, varying by less than 15 nm. The observed PL is related to the smaller $sp^2$ clusters of few aromatic rings or some other $sp^2$ configuration of similar size. All of the emission spectra were increased at first and then decrease of intensity as a result of gradual shifting of excitation wavelength. The coexistence of O and N in graphitized GCDs, which was demonstrated by the following FTIR and XPS analysis, brings about weak PL. Nitrogen doping would promote the efficiency of hole scavenging and hence dramatically enlarge the lifetime of the photogenerated electrons [33]. Furthermore, the increase of interconnectivity of the localized $sp^2$ sites facilitates hopping of photogenerated electrons to nonradiative recombination centres, and thus quenches PL [29]. These characteristics facilitate the separation of photoinduced electron-hole pairs, and consequently could promote the photocatalytic $CO_2$ reduction. The same conclusion was also identified by the lifetime of carriers, which would indirectly implied the electrons transfer in CDs. It can be reflected by the decays of PL transition centered on 425 nm excited at 270 nm as shown in Fig. 7c. Moreover, the PL lifetime of CDs calculated by the exponential analysis is also shown in the Table S2. The emission decay of CDs was three-exponential, suggesting that CDs have complex emitting center [26]. The PL lifetime decreases in the following sequence: GO-h-GCDs > CNT-h-GCDs > GH-i-ACDs ≈ GN-u-ACDs. A longer PL lifetime means lower recombination rate of the electron-hole pairs, which implied the more efficient electron transfer in CDs [34,35].

FTIR measurements were performed to determine detailed compositions and the functional groups in the as-synthesized CDs. As revealed in FTIR spectra (Fig. 8), there existed O—H, C=C, C=O, C=N, N—H, and C—O groups on the surface of CDs. Generally, two peaks at 1630 and 3470 $cm^{-1}$were attributed to C=O and O—H stretching vibrations respectively, and the peak at 1100 $cm^{-1}$ was associated with C—O bending vibrations [36]. Specifically, the FTIR spectrum reveals characteristic absorption bands of N—H and C=C stretching vibrations at 3420 and 2320 $cm^{-1}$ for GCDs [37]. To further clarify the components of the current CDs, X-ray photoelectron spectroscopy (XPS) spectra were performed. The XPS survey (Figs. 9a and Fig. S5a) shows three strong binding energy peaks at 281.18, 395.28 and 526.98 eV,

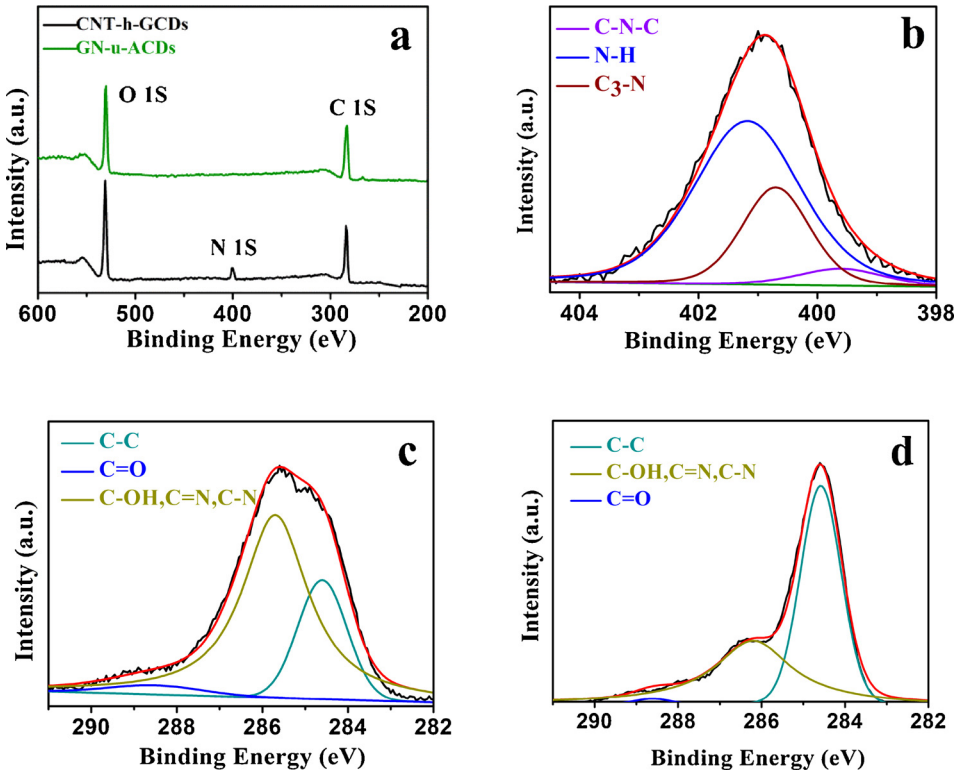


**Fig. 9.** XPS spectra of CDs, survey of GO-h-GCDs and GH-i -ACDs (a); N 1s of GO-h-GCDs (b); C 1s of GO-h-GCDs (c);C 1s of GH-i -ACDs (d).

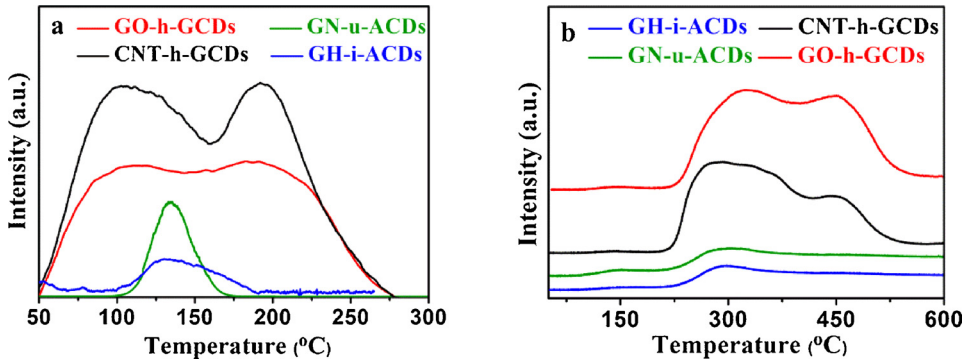


**Fig. 10.** $CO_2$-TPD (a) and CO-TPD (b) curves of GO-h-GCDs, CNT-h-GCDs, GN-u-ACDs and GH-i-ACDs.

attributed to $C_{1s}$, $N_{1s}$ and $O_{1s}$, respectively [38]. This result indicates that the GCDs are mainly composed of C, O and N, while ACDs are only consisted of two elements of C and O. The three binding energy peaks from small to large in $N_{1s}$ spectrum (Figs. 9b and S5c) are related to C—N—C, N-($C_3$) and N—H groups, respectively [39–41]. In the deconvoluted $C_{1s}$ spectrum, the binding energy at 284.6 eV represented C—C, and the peaks at about 286.0 eV represented C—N, C═N and C—OH. Additionally, the peaks at about 288.5 eV were related to C═O [42]. The XPS results confirmed the previous FTIR date, intensively suggesting that the GCDs were equipped with characteristic functional groups including pyridinic nitrogen, —COOH, —OH and small amount of —$NH_2$, and ACDs just contained —COOH and —OH which facilitated their excellent water solubility without extra chemical modification. More importantly, the basic nitrogen-containing groups could adsorb CO (the intermediate of $CO_2$ reduction), and this may play a key role in the high selectivity to $CH_4$ on GCDs photocatalyst.

$CO_2$ reduction reaction involves multiple proton-couple electron transfer and can result in the evolution of many different products depending on the adsorption and activation of $CO_2$ [43]. The $CO_2$-TPD experiments were performed as an attempt to evaluate the interaction difference between the $CO_2$ with ACDs and GCDs. In TPD, the desorption peak was on behalf of the adsorption type. The higher of desorption temperature is, the stronger of the interaction between adsorbate and surface adsorption site is. As shown in Fig. 10(a), the main desorption position was located at about 130 °C for ACDs and GCDs which was attributed to the interaction of $CO_2$ with surface hydroxyl groups of the sorbent [44]. Both GO-h-GCDs and CNT-h-GCDs exhibited broad peaks within the range 80–220 °C. The characteristic desorption peak of pyridinic rings centered at 105 °C and the desorption peaks of amine occurred at 190 °C [45,46]. The broad $CO_2$ desorption peak area of nitrogen-containing groups suggested more existence of basic sites which also coincided with hydroxyl groups to some extent.

As above, the photocatalysis products of all CDs include $H_2$ and CO, while GCDs also showed particular electron selectivity towards $CH_4$. Therefore, it can be supposed that the CO was served as a significant intermediate. To investigate the cause of differences in the selectivity, CO-TPD profiles of the CDs were tested and shown in Fig. 10(b). The desorption peak centred at 150 °C could be assigned to CO adsorbed by surface hydroxide groups. The peak at 280 °C might be ascribed to CO absorbed by aromatic rings. The graphitized GCDs with both the larger

$sp^2$ domains and the smaller $sp^2$ fragments showed stronger chemical adsorption than amorphous ACDs containing only finite-sized molecular $sp^2$ domains. The mainly difference in CO chemical adsorption is caused by surface nitrogen-containing groups, and the unique peak at 447 °C is the interaction between CO and surface nitrogen-containing groups. The intermediate CO can be easily desorbed from the surface of ACDs with weak CO chemisorptions, so $CO_2$ was just converted into CO on ACDs. On the surface of GCDs, the strongly adsorbed CO can accept excess electrons to form carbon radicals and subsequently combine with up to four H· radicals to form CH·, carbene, a methyl radical and eventually methane.

A possible photocatalytic $CO_2$ reduction mechanism could be proposed for better understanding the disparity in selectivity and rate between CDs on the basis of above. During the process, photogenerated electrons and holes would transfer to the surface of CDs, which act as a redox site and react with the adsorbed reactants. The localized $sp^2$ site and nitrogen-containing groups facilitate the separation of photogenerated electron-hole pairs and extend the lifetime of the photogenerated electrons significantly. At the same time, the surface hydroxide groups with moderate adsorption of hydrogen are likely to be responsible for the generation of $H_2$. The electrophilic C atom of $CO_2$ would interact with the surface electron centres (the nanometer-size $sp^2$ clusters and the finite-sized molecular $sp^2$ domains for GCDs and ACDs, respectively) or Lewis basic sites (surface nitrogen-containing groups) to form $CO_2\cdot^-$, which would react with adsorbed hydrogen to generate CO. The CO would be released from the surface of ACDs with weak CO adsorption properties and the product is CO. On GCDs, the strongly adsorbed CO could accept excess electrons to generate carbon radicals and subsequently to form methane.

## 4. Conclusions

CDs can serve as a photocatalyst to reduce stable $CO_2$ without metal loaded. The graphitized GCDs containing nitrogen-containing groups exhibited not only much higher rate of $CO_2$ reduction than ACDs, but also showed the ability to reduce $CO_2$ to $CH_4$ with 74.8% electronic selectivity. The preserved aromatic planes and nitrogen-containing groups of graphitized GCDs would improve the extraction of photogenerated charges for efficient photocatalysis, and the stronger CO chemisorption properties that induced by nitrogen-containing groups play a key role in methane-generating. The present study reveals the effect of nitrogen-containing groups and graphitization, which would be widely applicable to the CDs based composites with metal oxide or metal nanoparticles for photochemical degradation, photochemical synthesis and photochemical conversion.

## Acknowledgements

We acknowledge the financial support from National Natural Science Foundation of China (Nos. 91545116 and U1510108) and Pioneer “Hundred Talents Program” of CAS, Start-Up Grant of Institute of Coal Chemistry (2016SCXQT01).

## Appendix A. Supplementary data

Supplementary material related to this article can be found, in the online version, at doi:https://doi.org/10.1016/j.apcatb.2018.03.045.

## References

[1] C. Zhu, C. Liu, Y. Zhou, Y. Fu, S. Guo, H. Li, S. Zhao, H. Huang, Y. Liu, Z. Kang, Appl. Catal. B: Environ. 216 (2017) 114–121.
[2] H. Li, Z. Kang, Y. Liu, S.-T. Lee, J. Mater. Chem. 22 (2012) 24230.
[3] S. Thambiral, D. Ravi Shankaran, Appl. Surf. Sci. 390 (2016) 435–443.
[4] J. Zhou, P. Lin, J. Ma, X. Shan, H. Feng, C. Chen, J. Chen, Z. Qian, RSC Adv. 3 (2013) 9625.
[5] H. Li, R. Liu, S. Lian, Y. Liu, H. Huang, Z. Kang, Nanoscale 5 (2013) 3289–3297.
[6] J. Li, Y. Ma, Z. Ye, M. Zhou, H. Wang, C. Ma, D. Wang, P. Huo, Y. Yan, Appl. Catal. B: Environ. 204 (2017) 224–238.
[7] R. Wang, K.-Q. Lu, Z.-R. Tang, Y.-J. Xu, J. Mater. Chem. A 5 (2017) 3717–3734.
[8] H. Li, X. He, Z. Kang, H. Huang, Y. Liu, J. Liu, S. Lian, C.H. Tsang, X. Yang, S.T. Lee, Angew. Chem. 49 (2010) 4430–4434.
[9] H. Ding, H.-M. Xiong, RSC Adv. 5 (2015) 66528–66533.
[10] H. Zheng, Q. Wang, Y. Long, H. Zhang, X. Huang, R. Zhu, Chem. Commun. 47 (2011) 10650–10652.
[11] N. Serpone, A.V. Emeline, J. Phys. Chem Lett. 3 (2012) 673–677.
[12] B.C.M. Martindale, G.A.M. Hutton, C.A. Caputo, S. Prantl, R. Godin, J.R. Durrant, E. Reisner, Angew. Chem. 56 (2017) 6459–6463.
[13] Z. Luo, S. Lim, Z. Tian, J. Shang, L. Lai, B. MacDonald, C. Fu, Z. Shen, T. Yu, J. Lin, J. Mater. Chem. 21 (2011) 8038.
[14] F. Joucken, Y. Tison, J. Lagoute, J. Dumont, D. Cabosart, B. Zheng, V. Repain, C. Chacon, Y. Girard, A.R. Botello-Méndez, S. Rousset, R. Sporken, J.-C. Charlier, L. Henrard, Phys. Rev. B 85 (2012).
[15] S. Hu, R. Tian, L. Wu, Q. Zhao, J. Yang, J. Liu, S. Cao, Chem. Asian J. 8 (2013) 1035–1041.
[16] H. Tong, S. Ouyang, Y. Bi, N. Umezawa, M. Oshikiri, J. Ye, Adv. Mater. 24 (2012) 229–251.
[17] T.L. Thompson, J.T. Yates, Chem. Rev. 106 (2006) 4428–4453.
[18] R. Kuriki, H. Matsunaga, T. Nakashima, K. Wada, A. Yamakata, O. Ishitani, K. Maeda, J. Am. Chem. Soc. 138 (2016) 5159–5170.
[19] W.-J. Ong, L.K. Putri, L.-L. Tan, S.-P. Chai, S.-T. Yong, Appl. Catal. B: Environ. 180 (2016) 530–543.
[20] J.C. Wang, H.C. Yao, Z.Y. Fan, L. Zhang, J.S. Wang, S.Q. Zang, Z.J. Li, ACS Appl. Mater. Interfaces 8 (2016) 3765–3775.
[21] H. Li, X. Zhang, D.R. MacFarlane, Adv. Energy Mater. 5 (2015).
[22] L. Cao, S. Sahu, P. Anilkumar, C.E. Bunker, J. Xu, K.A.S. Fernando, P. Wang, E.A. Guliants, K.N. Tackett, Y.-P. Sun, J. Am. Chem. Soc. 133 (2011) 4754–4757.
[23] H. Li, R. Liu, Y. Liu, H. Huang, H. Yu, H. Ming, S. Lian, S.-T. Lee, Z. Kang, J. Mater. Chem. 22 (2012) 17470.
[24] X. Wang, D. Wang, Y. Guo, C. Yang, A. Iqbal, W. Liu, W. Qin, D. Yan, H. Guo, Dalton Trans. 44 (2015) 5547–5554.
[25] J. Gao, C. Xu, Y. Hu, F. Zhao, C. Shao, Y. Zhao, S. Chen, L. Qu, Chem. Asian J. 12 (2017) 1272–1276.
[26] T. Shimidzu, T. Iyoda, Y. Koide, J. Am. Chem. Soc. 107 (1) (1985) 35–41.
[27] J.C. Meyer, A.K. Geim, M.I. Katsnelson, K.S. Novoselov, T.J. Booth, S. Roth, Nature 446 (2007) 60–63.
[28] Y. Hu, P. Wu, Y. Yin, H. Zhang, C. Cai, Appl. Catal. B: Environ. 111–112 (2012) 208–217.
[29] G. Eda, Y.Y. Lin, C. Mattevi, H. Yamaguchi, H.A. Chen, I. Chen, C.W. Chen, M. Chhowalla, Adv. Mater. 22 (2010) 505–509.
[30] C. Mattevi, G. Eda, S. Agnoli, S. Miller, K.A. Mkhoyan, O. Celik, D. Mastrogiovanni, G. Granozzi, E. Garfunkel, M. Chhowalla, Adv. Funct. Mater. 19 (2009) 2577–2583.
[31] C. Mathioudakis, G. Kopidakis, P.C. Kelires, P. Patsalas, M. Gioti, S. Logothetidis, Thin Solid Films 482 (2005) 151–155.
[32] C.W. Chen, J. Robertson, J. Non-Cryst. Solids 227 (1998) 602–606.
[33] B. Martindale, G.A. Hutton, C.A. Caputo, S. Prantl, R. Godin, J.R. Durrant, E. Reisner, Angew. Chem. Int. Ed. 56 (2017) 6459–6463.
[34] Z. Li, B. Tian, W. Zhang, X. Zhang, Y. Wu, G. Lu, Appl. Catal. B: Environ. 204 (2017) 33–42.
[35] B. Liu, L. Peng, J. Alloys Compd. 571 (2013) 145–152.
[36] X. Yang, Y. Zhuo, S. Zhu, Y. Luo, Y. Feng, Y. Dou, Biosens. Bioelectron. 60 (2014) 292–298.
[37] L. Lin, M. Rong, S. Lu, X. Song, Y. Zhong, J. Yan, Y. Wang, X. Chen, Nanoscale 7 (2015) 1872–1878.
[38] C. Zhou, X. He, D. Ya, J. Zhong, B. Deng, Sens. Actuators B: Chem. 249 (2017) 256–264.
[39] S. Liu, J. Tian, L. Wang, Y. Zhang, X. Qin, Y. Luo, A.M. Asiri, A.O. Al-Youbi, X. Sun, Adv. Mater. 24 (2012) 2037–2041.
[40] W. Li, Z. Zhang, B. Kong, S. Feng, J. Wang, L. Wang, J. Yang, F. Zhang, P. Wu, D. Zhao, Angew. Chem. 52 (2013) 8151–8155.
[41] L. Shi, L. Li, X. Li, G. Zhang, Y. Zhang, C. Dong, S. Shuang, Sens. Actuators B: Chem. 251 (2017) 234–241.
[42] B. Singh, Y. Fang, B.C.C. Cowie, L. Thomsen, Org. Geochem. 77 (2014) 1–10.
[43] X. Chang, T. Wang, J. Gong, Energy Environ. Sci. 9 (2016) 2177–2196.
[44] Z.Z. And, T.J. Pinnavaia, J. Am. Chem. Soc. 124 (2012) 12294–12301.
[45] D. Tiwari, H. Bhunia, P.K. Bajpai, RSC Adv. 6 (2016) 111842–111855.
[46] S. Xian, J. Peng, Z. Zhang, Q. Xia, H. Wang, Z. Li, Chem. Eng. J. 270 (2015) 385–392.